PREPRINT UCRL-82684

CONF-790674--1

Lawrence Livermore Laboratory

Micro-Fresnel Structures for Microscopy of Laser Generated Bright X-ray Sources

N. M. Ceglio, University of California, Lawrence Livermore Laboratory

and

D. C. Shavers, D. C. Flanders and H. I. Smith
Massachusetts Institute of Technology, Lincoln Laboratory

June 5, 1979

Prepared for Presentation as an Invited Paper at the New York Academy of Sciences Conference on Ultrasoft X-ray Microscopy, June 13-15, 1979, New York, N.Y.

Micro-Fresnel Structures for Microscopy of Laser Generated Bright X-ray Sources

I. Characteristics of and Model for Laser Generated Bright X-ray Sources:

X-ray microscopists have historically been interested in novel ways of producing bright x-ray sources. One such method for producing same is to focus an intense laser beam onto a microscopic high Z (atomic number) target. The characteristics of the emission from such a microscopic source, and a simplified model of the physical processes involved, are briefly described in the following paragraphs.

Figure 1 illustrates the laser-target parameters under consideration here. A gold micro-disk, 500 μm in diameter, 15 μm thick is irradiated with 1.06 μm laser light at an intensity of $\sim 3 \times 10^{14}$ watts/cm^2. The laser pulse width is 1 nsec, the pulse energy $\sim$ 450 joules. A detailed analysis of the laser-target interaction physics leading to x-ray emission under these conditions is a matter of some complication, and is being actively pursued by a number of investigators.[1] However, such a detailed analysis is unnecessary here. The major features of x-ray emission from such a target can be adequately characterized by a very simple model.

X-ray source parameters of interest to an x-ray microscopist are source spectrum, temporal duration, spatial extent, angular distribution, and x-ray conversion efficiency. These parameters have all been measured for the laser-target conditions specified, and measured data are presented in Figure 1. A remarkably good fit to the measured x-ray results can be obtained by simply treating the laser-target interaction as producing a microscopic, equilibrium plasma of temperature kT, determined by a macroscopic energy balance.[2] The plasma radiates as a blackbody at temperature kT thereby accounting for the

shape of the measured spectrum (Figure 2). The duration of emission is determined by the hydrodynamic disassembly[3] and radiation cooling of the plasma. This leads to an x-ray emission duration roughly 1 to 2 times the laser pulse wioth for 1 nsec pulses. The spatial extent of the microscopic x-ray source is roughly the plasma expansion size during the 1-2 nsec emission period, i.e. a plasma cylinder $\sim$ 50 μm diameter, $\sim$ 100 μm thick. Treating the "plasma cylinder" as an optically thick x-ray source is sufficient to account for the observed angular distribution from the laser generated source. The x-ray emission angular distribution is found to be a broad lobe in the forward direction (i.e. back toward the incident laser beam) (with roughly 4-5 times as much emission (joules/Sr) in the forward direction as out to the side (i.e. normal to the incidient laser beam).

This simple model for the laser generated x-ray source as a microscopic equilibrium plasma radiating as a blackbody for a finite time determined by its hydrodynamic disassembly and radiation losses, although adequate for a description of the spectrum, duration, size and angular distribution of the x-ray emission, cannot easily provide quantitative clues to laser light absorption and x-ray conversion efficiency in such experiments. It is generally found that for the laser-target parameters under consideration roughly 50% of the incident laser light is absorbed and roughly 36% of the absorbed energy is radiated in the x-ray band from 100-1500 eV.

II. X-ray Microscopy of Laser Generated Microscopic Plasmas

At the Lawrence Livermore Laboratory, we are focussing intense laser beams onto microscopic targets not to produce x-ray sources for microscopy, but instead to ignite thermonuclear reactions on a microscopic scale. Our typical

target in this effort is a Deuterium-Tritium (D-T) filled glass microsphere (Fig. 3), not a gold microdisk. The x-ray emission from such laser irradiated microspheres serves as an important diagnostic aid to the understanding of the physical processes occurring in these targets. X-ray microscopy of these self luminous sources has therefore been a high priority in our program and a number of complementary techniques have been developed.

A. Broadband Techniques; 3 μm - 10 μm Resolution

Grazing Incidence Reflection (GIR) x-ray microscopes of the Kirkpatrick-Baez design (orthogonal, cylindrical mirror pairs) are being routinely used to produce x-ray images with 3-5 μm resolution of laser irradiated targets.[4] As illustrated in Fig. 4 the instrument is typically used with four separate spectral channels (each having $\Delta E/E \simeq 0.3$) ranging from .6 keV up to 3.5 keV.

Spectral discrimination is achieved by varying mirror surface materials and filter foils in the different spectral channels. Imaging characteristics of these microscopes are summarized below:

Effective Solid Angle :	2×10^{-7} sr.
Resolution :	3 - 5 μm
Field of View (for 3-5 μm resolution)	500 μm
Spectral Range :	.6 keV - 3.5 keV
Magnification :	3X

In addition to GIR x-ray microscopy, coded imaging techniques employing Fresnel zone plates as coded apertures are being used to provide 5 - 10 μm resolution images of higher energy (3 - 50 keV) x-ray emissions from laser irradiated targets.[5] Figure 5 illustrates the principles of Zone Plate Coded Imaging (ZPCI). ZPCI is a broadband, two step imaging technique. In the first step the x-ray source to be imaged casts a shadowgraph (coded image) through a

Fresnel zone plate (coded aperture) onto photographic film. Image reconstruction (decoding) is achieved via procedures similar to those used in holography. The shadowgraph is illuminated with a coherent light source. The Fresnel diffraction pattern of the transmitted light produces a reconstruction of the original source distribution - inverted and magnified.

Coded imaging techniques serve as a useful complement to GIR techniques in x-ray microscopy of laser fusion targets. They provide moderate resolution capability (5 - 10 μm), over a large field of view (centimeters), with a broad spectral capability (Δ E/E ≈ .5 over 3 - 50 keV), with large effective solid angle (10^{-2} - 10^{-1} sr). Coded imaging techniques are limited, however, to sources having an active area << coded aperture area. Since we currently fabricate micro-Fresnel zone plate coded apertures having diameters as large as 15 mm, this limitation is of no consequence for the microscopy of laser fusion targets.

Imaging characteristics of the Zone Plate Coded Imaging technique are summarized below:

Effective Solid Angle :	10^{-2} - 10^{-1} sr.
Resolution :	5 - 10 μm
Field of View :	centimeters
Spectral Range :	3 keV - 50 keV
Limitation :	Source Active Area << Coded Aperture Area

Typical x-ray images of laser fusion targets using the GIR x-ray microscope and the ZPCI technique are shown in Fig. 6.

B. Narrowband Techniques; Submicron Resolution:

In addition to our need for broadband ($\frac{\Delta E}{E} \sim .3$ - .5), moderate resolution (3 -10 μm) microscopic techniques, there is a strong interest within the laser fusion program (as well as other fields) for narrowband ($\frac{\Delta E}{E} \sim 10^{-2}$)

x-ray optical components having submicron resolution and large solid angle for radiation collection. In pursuit of this interest we have designed an efficient x-ray lens[5], and have embarked on a long term program for the fabrication and testing of such lensing elements.

Quantitative details of the x-ray lens design are presented elsewhere[6], a brief qualitative description of its underlying principles follows. The x-ray lens may be described as a transmission Blazed Fresnel Phase Plate (BFPP). A BFPP is a Fresnel zone structure with a spatially distributed phase shift within each Fresnel zone. The spatial distribution of the phase shifts is chosen to concentrate essentially all of the unabsorbed energy into a single focal spot. Figures 7(a), (b), (c) illustrate the BFPP concept in three stages; these stages also correspond to the chronolgy of our x-ray lens fabrication effort. Figure 7(a) shows a Fresnel Zone Plate. The FZP performs an amplitude modulation (periodic in r^2) of the incident plane wave, focusing roughly 10% of the incident energy into a first order focal spot. Figure 7(b) shows a Fresnel Phase Plate, a somewhat more efficient focusing element. The FPP performs a phase and amplitude (because of finite x-ray absorption) modulation of the incident plane wave. The modulation function has the form of a square wave periodic in r^2. In the limit of small absorption the FPP can focus roughly 40% of the incident energy into a first order focal spot. Figure 7(c) shows a Blazed Fresnel Phase Plate. The BFPP transforms the incident plane wave into a converging spherical wave having an amplitude modulation (because of finite x-ray absorption) which is periodic in r^2. As a result of the periodic amplitude modulation, the BFPP will diffract energy into foci other than the first order real focus. However, in cases of small absorption such effects are negligible and practically all the unabsorbed energy is directed into the first order real focus.

The expected resolution for such an x-ray lens would be roughly equal to the width of the minimum zone. We anticipate the fabrication of x-ray lensing elements with linewidths ranging from 1000 Å to 4000 Å for use over an x-ray wavelength range from 1.5 Å - 500 Å. Table 1 provides a calculated evaluation of the efficiency of proposed x-ray lensing elements fabricated from practical materials, having linewidths ranging over 1000 Å to 4000 Å, intended for use at wavelengths ranging from 1.5 Å to 500 Å. In this table 'F' is the fraction of energy emitted by an isotropic, monochromatic point source which can be collimated into a parallel beam by the x-ray lens. It takes into account x-ray absorption by the lens material, diffraction into "wasted" orders, and the finite numerical aperture of the lens. '$f_{\varepsilon}^{\#}$' is the effective f/number of the x-ray lens taking into account diffraction and absorption losses.

The fabrication effort for production of efficient x-ray lensing elements has been divided into three phases along the lines of the staged discussion in Figs. 7(a), (b), (c). The first phase involves the fabrication of thick (1 - 1.5 μm), gold micro-Fresnel zone plates having linewidths from 1000 Å - 4000 Å. The second phase involves the fabrication of phase plates of similar dimensions of appropriately selected materials. In the final phase precision blazing of the micro-Fresnel structures will be attempted. Fabrication of these micro Fresnel structures using electron beam and x-ray lithographic techniques is being carried out at the Massachusetts Institute of Technology, Lincoln Laboratory.[7] Evaluation and x-ray testing of the lensing elements is being carried out at the University of California, Lawrence Livermore Laboratory.

We are currently involved in the first phase of the three phase fabrication and testing program outlined above. Micro-Fresnel zone plates of 1.5 μm thick gold, 3200 Å minimum linewidth, .632 mm diameter have been fabricated. Preliminary testing of the imaging characteristics (resolution, field of view, depth

of field) has begun. Figure 9 illustrates the test set up in which the zone plate "lens" is used as the optical component of a 4X microscope. In this experiment the lens is used to image a 1 mm diameter crude (2.5 μm minimum linewidth) Fresnel zone plate used as a test mask.[8] The zone plate acts as an ideal resolution test pattern, since the linewidths vary predictably over a wide range. The test pattern is backlit with Al K_α radiation at λ = 8.34 Å produced by irradiating a water cooled aluminum target with a 2.5 Mev, 50 μ amp proton beam from a Van deGraff generator. The x-ray images are recorded on single sided type M x-ray film. A representative x-ray image of the 2.5 μm linewidth test pattern is shown in Fig. 9. It can be seen that the outermost zones of the test pattern are resolved. This is more clearly illustrated in the data of Fig. 10 in which the x-ray image has been scanned by a PDS microdensitometer and the radial density distribution over the outermost 20 dark zones (from "A" to "B") plotted. The individual zones are clearly resolved, while modulations in the image density level produced by nonuniformity of the backlighting source and spatial shot noise in the image can also be seen. A zone plate test pattern mask having minimum linewidth $\lesssim$ 1 μm is currently being fabricated to extend the resolution tests into the submicron regime. Additional simple tests of the zone plate lens field of view and depth of focus (in the image plane) were made by translating the test mask off the optical axis ($\pm$ 1 mm) and by varying the image plane position ($\pm$ 20 mm). As expected, these variations had no affect on the ability of the lens to resolve the 2.5 μm lines of the test pattern.

Also included in the first phase of this x-ray lens development program is the fabrication and testing of off-axis micro-Fresnel zone plates to be used as imaging spectrometers for polychromatic x-ray sources. The imaging characteristics of an off-axis Fresnel zone plate are illustrated in Fig. 11. The off-

axis zone plate is simply a circular, off-axis segment of a circularly symmetric (on-axis) Fresnel zone plate. The off-axis zone plate has the same focal length as its "parent" on-axis zone plate ($f = \frac{r_1^2}{\lambda}$) and similar chromatic aberrations. However, due to its off-axis geometry there exists the possibility of spatially separating chromatically distinct emissions from the same source, thereby providing multiple, two dimensional, chromatically distinct images of a polychromatic source (Fig. 11).

In order for an imaging spectrometer, employing an off-axis zone plate as its optical element, to successfully separate spectrally distinct images from a given source, certain design criteria impacting both the source and the instrument must be met. Using simple ray tracing calculations, we arrive at the following qualitative criteria:

spectral lines (λ_1, λ_2, ...) must be well separated

source size (in the offset direction) must not be too large

zone plate offset distance must be sufficiently large ($r_o < \Delta_o < 2\ r_o$)[9],

and minimum linewidth as small as possible.

An example of an imaging spectrometer design employing off-axis zone plates currently being fabricated for use with laser fusion targets is presented below:

mimimum zone width :	$\Delta r = 1600$ Å
off-axis zone plate radius :	$r_o = .375$ mm
offset distance :	$\Delta_o = .5$ mm
spectral lines :	$\lambda_1 \simeq 4$ Å, $\lambda_2 \simeq 6.9$ Å
max source size for separable images :	$S \simeq 500$ μm

A practical consideration for the imaging spectrometer is the apparent need for microscopic recording media to capture the separated images without blocking shorter wavelength images to be recorded downstream (see Fig. 11). This problem can be obviated and macroscopic recording media used if the imaging planes for the long wavelength images are appropriately tilted back toward the horizontal. The maximum angle of tilt toward the horizontal is limited by the depth of focus (in the image plane) and can be determined from simple calculations. For the example cited above the maximum tilt angle is roughly 81.5° yielding a recording-medium width $\simeq 2.5$ mm for the image at $\lambda = 6.9$ Å.

Off-axis zone plates used as imaging spectrometers will very likely find a wide range of application in the laser fusion program (and other fields as well). In the particular example cited above the spectral lines chosen are the Argon and Silicon K_α emissions from the multiply ionized laser fusion target. The Argon is added as a tracer element in the D-T fuel, and the Silicon is a natural constituent of the glass microsphere. The imaging spectromenter will, therefore, provide separate and distinct images of the glass pusher and the enclosed fuel during the laser driven target implosion.

III. Summary:

A brief parametric survey of the x-ray characteristics of a gold micro-disk irradiated at 3×10^{14} watt/cm^2 by a 1 nsec Nd-glass laser pulse has been provided as an example of a laser generated bright x-ray source. It was shown that a simple phenomenological model of the laser generated x-ray source as a microscopic equilibrium plasma radiating as a blackbody for a finite time determined by its hydrodynamic disassembly and radiation losses, serves to provide an adequate approximation to the x-ray characteristics of such sources.

The current state of x-ray microscopy within the LLL laser fusion program was briefly reviewed. Kirpatrick-Baez grazing incidence reflection x-ray microscopes are being used to provide 3-5 μm resolution, broadband images ($\frac{\Delta E}{E} \sim 0.3$) over a spectral range from .6 keV to 3.5 keV. Zone Plate Coded Imaging is used to provide 5-10 μm resolution, broadband ($\frac{\Delta E}{E} \sim 0.5$) images over a spectral range from 3 keV to 50 keV. Efficient x-ray lensing elements with anticipated submicron resolution are being developed for narrowband ($\frac{\Delta E}{E} \sim 10^{-2}$) imaging applications over a spectral range .1 keV - 8 keV. The x-ray lens design is that of a transmission blazed Fresnel phase plate. We are currently in the earliest stages of the x-ray lens development effort. Micro-Fresnel zone plates with 3200 Å minimum linewidth have been fabricated and preliminary resolution tests begun. The first resolution test pattern, having minimum linewidth of 2.5 μm, was imaged in $\lambda = 8.34$ Å light with no difficulty. Newer test patterns with submicron minimum line are being prepared for the next stage of resolution testing. An off-axis Fresnel zone plate with 1600 Å minimum linewidth is presently being fabricated for use as an imaging spectrometer in order to provide spatially separated, chromatically distinct images of characteristic line emissions from laser fusion targets.

Acknowledgements:

The authors wish to acknowledge the significant contributions provided by their colleagues: H. G. Ahlstrom and L. W. Coleman for their enthusiastic support of a broad based, diversified x-ray microscopy effort within the laser fusion program; D. T. Attwood for useful technical discussions of laser-plasma interaction physics; D. L. Matthews, R. J. Fortner and D. Gaines for their assistance in x-ray lens resolution test experiments; M. J. Boyle and R. H. Price for providing grazing incidence reflection x-ray microscope data; and G. L. Howe and W. T. Tiffany for the fabrication and assembly of the 4X test microscope used in resolution test experiments.

References

1. R. A. Haas, et al., Phys. Fluids 20, 322 (1977); H. D. Shay et al., Phys. Fluids 21, 1634 (1978); M. D. Rosen, et al. Lawrence Livermore Laboratory Report No. UCRL-82146 (submitted to Phys. Fluids).

2. Determination of the equilibrium plasma temperature is not as simple as implied. In fact it may be more accurate to treat kT as a free parameter fitted to the shape of the measured x-ray spectrum (i.e. peak of spectrum = 2.82 kT). A true energy balance must account for: the fractional absorption of the incident laser energy ($\sim$ 50%), energy loss by radiation ($\sim$ 36% of that absorbed); the degree of ionization of the plasma ($Z^* \simeq 30$, not accurately known); the average ionization potential per removed electron. In addition, if a very thin target is chosen (or longer laser pulse) significant expansion cooling may occur during irradiation, or if a very thick target is used then only a fraction of the target mass becomes ionized and detailed heat conduction processses between the plasma and the larger target mass will play an important role in the overall energy balance. All these details notwithstanding one can get a good guess at kT in our case using the following rule of thumb: divide the total absorbed energy (225 joules) by the total number of free particles ((Z^*+1) x number of atoms) and equate this to 3/2 kT.

3. The exploding microdisk will expand at the ion sound speed where

$$V_s \simeq \left(\frac{\gamma_i \, kT_i + \gamma_e \, Z^* \, kT_e}{Mi} \right)^{1/2}$$

$\gamma i \simeq 3$, $\gamma_e \simeq 1$; $Z^* \simeq 30$; $Te = Ti = 177$ eV; $M_i \simeq 3.3 \times 10^{-25}$ gm in our simple model.

4. F. Seward, et al., Rev. Sci. Instr. 47, 464 (April 1976).

5. N. M. Ceglio, D. T. Attwood, and E. V. George, J. Appl. Phys, 48, 1566 (April, 1977); N. M. Ceglio, Proceedings SPIE, Vol 106: X-Ray Imaging, p. 55 (1977).

6. N. M. Ceglio and Henry I. Smith, Proceedings of VIII International Conference on X-Ray Optics and Microanalysis, Boston, (August, 1977).

7. D. C. Shavers, et al., Proceedings of Fifteenth Symposium on Electron, Ion, and Photon Beam Technology, Boston, (May, 1979). (To be published in J. Vac. Sci. Tech., Nov. - Dec., 1979).

8. The crude zone plate used as the test pattern mask is one of the coded apertures routinely used in the ZPCI work.

9. The criterion $r_o < \Delta_o < 2r_o$ requires further explanation. $r_o < \Delta_o$ is necessary for optimization of image separation in the spectrometer $\Delta_o < 2r_o$ is necessary to maintain finite optical transfer function (OTF) response at low spatial frequencies for the off-axis zone plate. If the offset distance (Δ_o) significantly exceeds the zone plate diameter ($2r_o$) the off-axis zone plate will exhibit a spatial frequency "pass band" response making it sensitive to very small objects (High spatial frequencies) but insensitive to larger objects (low spatial frequencies) within its field of view.

Figure Captions

Fig. 1 For the laser-target parameters illustrated, a simple model is adequate to characterize the laser generated x-ray source. The source is viewed as a microscopic equilibrium plasma radiating as a blackbody for a finite time determined by its hydrodynamic disassembly and radiation losses. For this microscopic x-ray source roughly 18% of the incident laser energy is converted into x-rays in the 100 eV - 1500 eV spectral band; the duration of emission is 1 - 2 nsec; and the angular distribution of emission is roughly that from an optically thick disk 100 μm thick, 500 μm diameter.

Fig. 2 Measured x-ray spectrum from a gold microdisk irradiated at 3×10^{14} watt/cm^2 by a Nd-glass laser. The measured spectral shape is matched reasonably well by that from a blackbody with kT = 177 eV.

Fig. 3 Typical D-T filled glass microsphere laser fusion target

Fig. 4 Kirkpatrick-Baez design (orthogonal, cylindrical mirror pairs) grazing incidence reflection x-ray microscope operating in four spectral channels determined by K edge filter foils and mirror surface materials.

Fig. 5 Basic principles of the two-step ZPCI technique. Step 1: a zone-plate shadow camera views the imploding target. The emitted radiation appropriately filtered--casts a shadow through a Fresnel-zone-plate aperture onto a recording film. Each source point will cast a separate shadow onto the recording film, producing a shadowgraph. Each zone-plate shadow uniquely characterizes, by its size and position, the spatial position of its associated point. Step 2: the processed shadowgraph transparency is illuminated with a low-power, visible-light laser beam. Each zone-plate shadow focuses the incident laser light to a diffraction-limited spot--the inversely located image of its associated source point.

Fig. 6 (a) x-ray image of a laser imploded microsphere target taken with a grazing incidence reflection x-ray microscope. Image resolution is 3 μm. Emission from the glass shell occurs during the initial laser irradiation of the target. The large bright spot at image center is emission from the symmetrically imploded D-T fuel.

(b) x-ray image (similar to (a)) of a laser imploded microsphere target taken using the two step zone plate coded imaging (ZPCI) technique. Image resolution is ≃ 8 μm.

Fig. 7 Staged illustration of the x-ray lens (transmission blazed Fresnel phase plate) concept. (a) shows the energy distribution for a parallel monochromatic beam incident on a Fresnel zone plate. (b) illustrates the energy distribution under the same conditions for a Fresnel phase plate. Note that for small absorption ($\Gamma \to 1$) the undiffracted component approaches zero while approximately 40% of the incident radiation is diffracted into the first order real focus. (c) illustrates a blazed Fresnel phase plate with quadratic phase modulation in adjacent pairs of Fresnel zones. Note that for small absorption ($\eta \to 0$, $\Gamma \to 1$) all the incident radiation is diffracted into the first order real focus.

Fig. 8 Resolution tests of a Fresnel zone plate x-ray lensing element are conducted on a rigid optical bench set up. The lensing element being tested has a minimum linewidth of 3200 Å, thickness = 1.5 μm gold, and a .632 mm diameter. It is used to image a free standing, crude Fresnel zone plate with 2.5 μm minimum zone width backlit by an Aluminum K_α x-ray source. The radial strut patterns on both the zone plate lens and the zone plate test pattern are used to support these free standing, gold microstructures.

Fig. 9 Initial resolution tests of the zone plate lens were conducted using a test pattern with minimum linewidth of 2.5 μm even though the anticipated resolution of the instrument is roughly 0.5 μm. The 2.5 μm outermost lines of the test pattern were easily resolved

Fig. 10 The ability of the zone plate lens to clearly resolve the 2.5 μm minimum lines of the test pattern is illustrated by a microdensitometer analysis of the x-ray image. A microdensitometer scan from "A" to "B" across the outermost twenty dark zones of the image shows the individual zones to be clearly resolved.

Fig. 11 An off-axis segment of a Fresnel zone plate can be used as an imaging spectrometer to spatially separate distinct spectral emissions from a polychromatic source as illustrated.

Table I

X-RAY LENS EFFICIENCY CALCULATIONS

Material	Wavelength λ	Min modulation width $2\Delta r$	Collection fraction F	Effective f/number $f^{\#}_{\varepsilon}$
Aluminum	10 Å	1000 Å	1.8×10^{-5}	58
	25 Å	1000 Å	1.6×10^{-4}	36
	500 Å	4000 Å	2.3×10^{-3}	5
Polystyrene	67 Å	1000 Å	8.3×10^{-4}	7.5
	150 Å	2000 Å	5.0×10^{-4}	11
Silicon	24 Å	1000 Å	4.2×10^{-5}	38
Gold	1.5 Å	1000 Å	2.9×10^{-7}	462

A pair of parameters used to estimate x-ray lens efficiency are tabulated for a number of practical lens materials, minimum zone pair width, and imaging wavelength. F and $f^{\#}_{\varepsilon}$ are calculated assuming a monochromatic point source placed in the focal plane of the lens, taking into account all absorption and diffraction losses.

- ADDENDUM -

The authors wish to add that during the preparation of this manuscript the x-ray lens resolution tests using a test pattern with 1 μm lines (as discussed on p. 7) were completed. The x-ray lens successfully resolved the 1 μm lines of the test pattern. Further testing is continuing.

LASER GENERATED BRIGHT X-RAY SOURCE — A SIMPLIFIED VIEW:

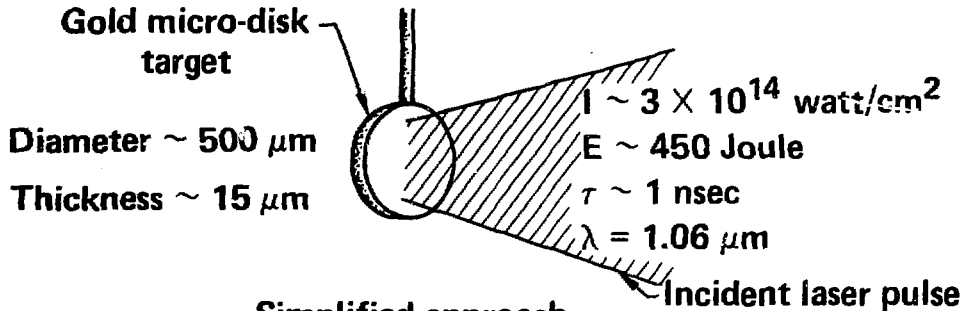

— Simplified approach —

X-ray source	Plasma at temp. kT determined by simple energy balance ($kT \simeq 177$ eV)
X-ray spectrum	Blackbody radiation at temp. kT { Spectral band 100 eV — 1500 eV dominates }
Emission duration	Cooling down time of plasma (expansion cooling and radiation cooling) ($\tau \approx 1 - 2$ nsec)
Spatial size	Plasma expansion size during emission (disk $\approx 500\ \mu m \times 100\ \mu m$)
X-ray conversion efficiency	Empirical ($\eta \approx 18\%$ of incident laser energy)

40-90-0579-1779

Fig. 1

LASER GENERATED BRIGHT X-RAY SOURCE – MEASURED SPECTRUM:

Time integrated x-ray emission in forward (2 π) direction:

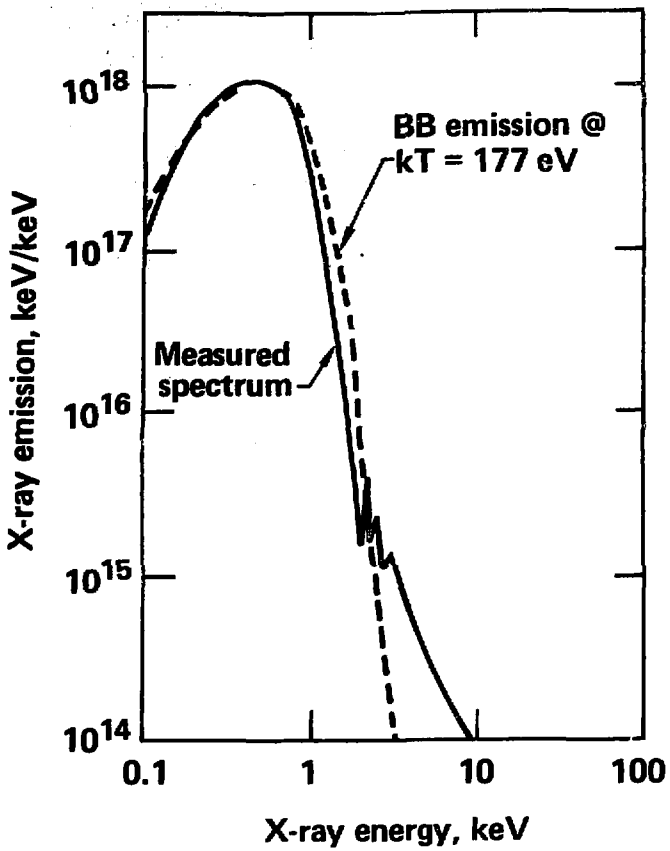

40-90-0579-1778

Parameters:

$I \simeq 3 \times 10^{14}$ watt/cm^2

$\tau \simeq 1$ nsec

$\lambda \simeq 1.06$ μm

Gold disk: Diameter ~ 500 μm

Thickness ~ 15 μm

Fig. 2

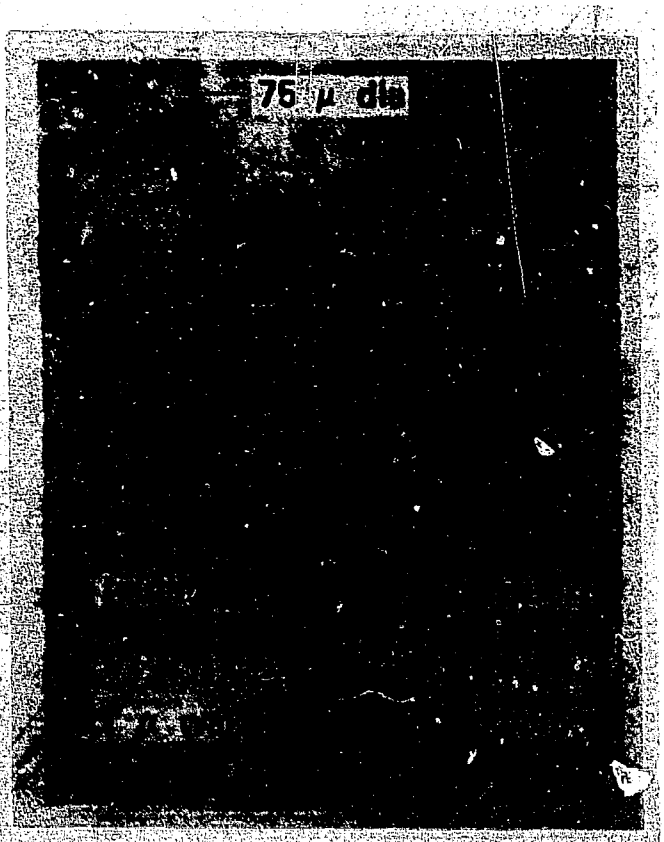

Fig. 3

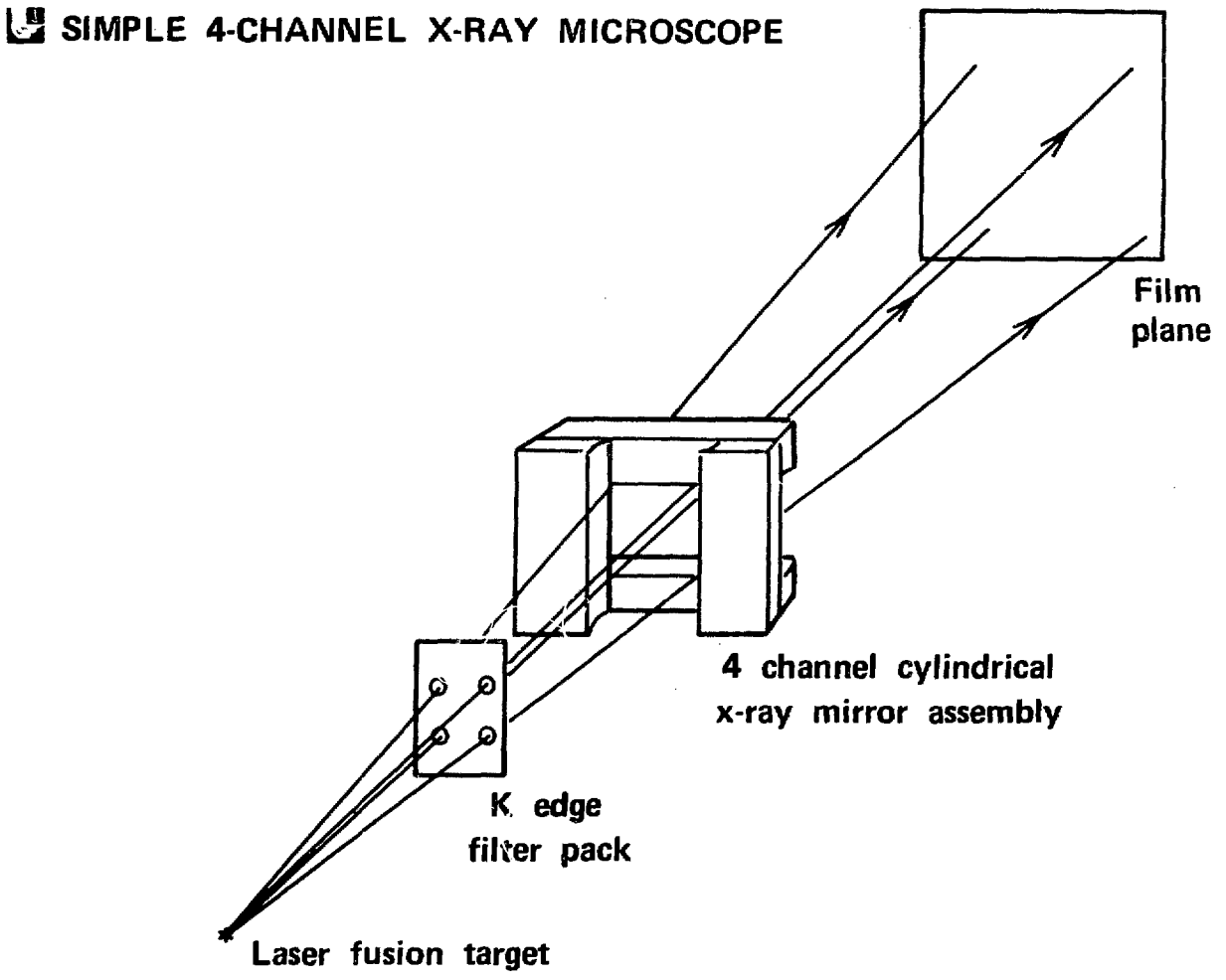
SIMPLE 4-CHANNEL X-RAY MICROSCOPE
Film plane
4 channel cylindrical x-ray mirror assembly
K edge filter pack
Laser fusion target

Fig. 4

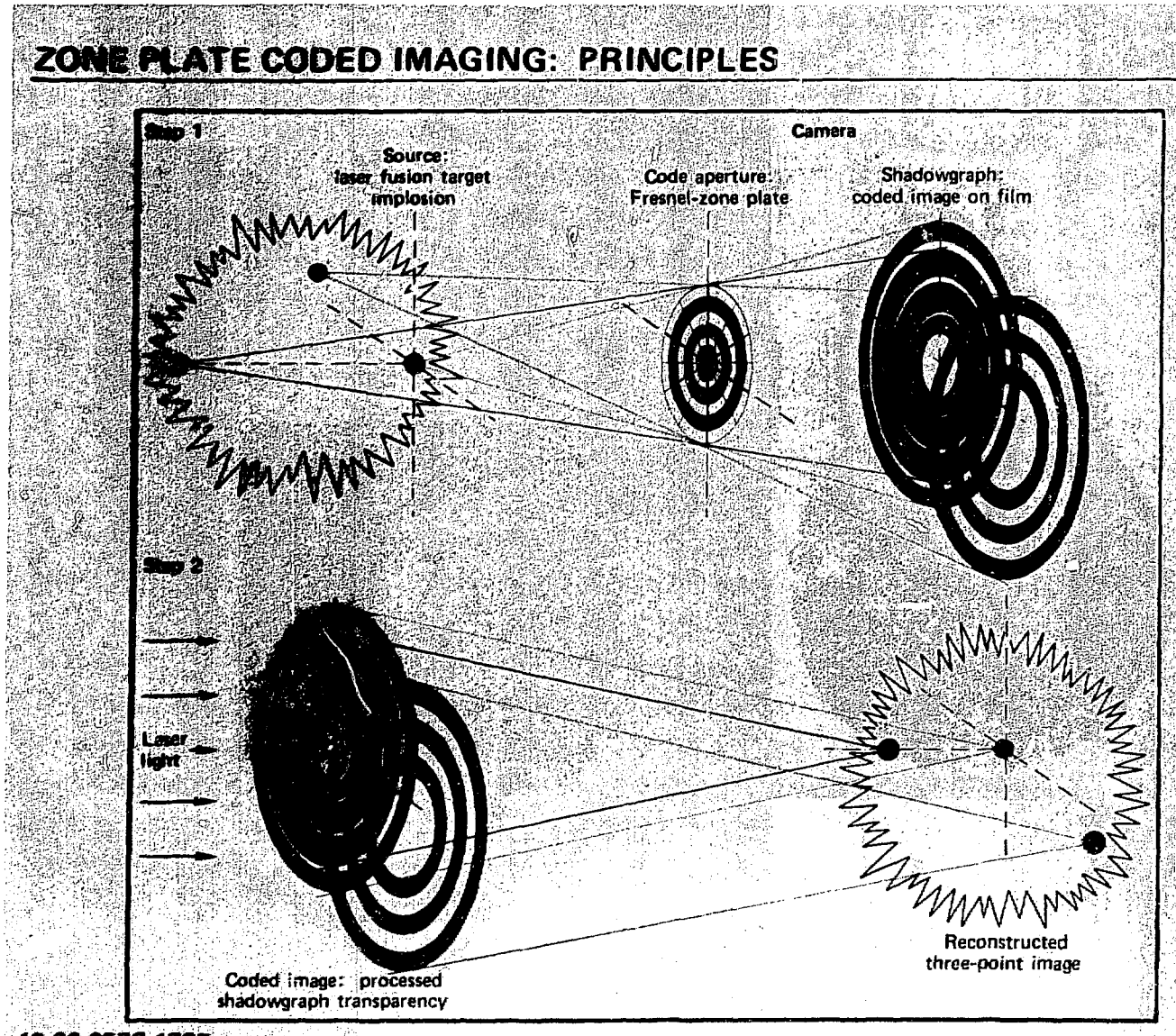
ZONE PLATE CODED IMAGING: PRINCIPLES
Step 1
Source:
laser fusion target
implosion
Camera
Code aperture:
Fresnel-zone plate
Shadowgraph:
coded image on film
Step 2
Laser
light
Coded image: processed
shadowgraph transparency
Reconstructed
three-point image
40-90-0578-1795

Fig. 5

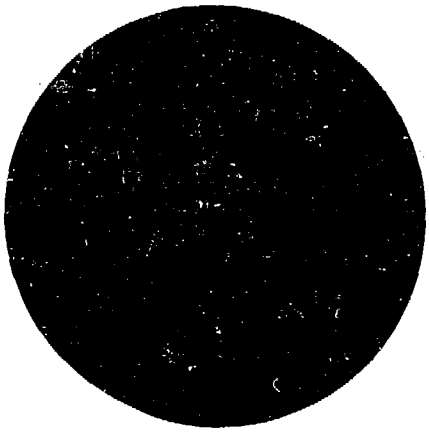

(a)

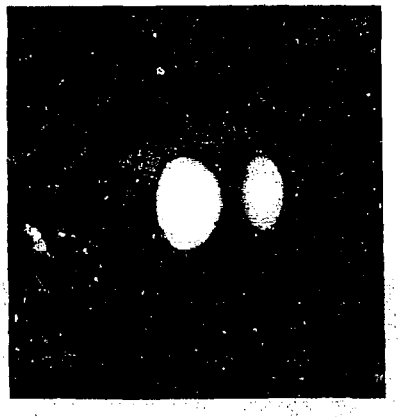

(b)

Fig. 6

WHAT IS A BLAZED FRESNEL PHASE PLATE?

Illustration in stages: (1) Fresnel zone plate

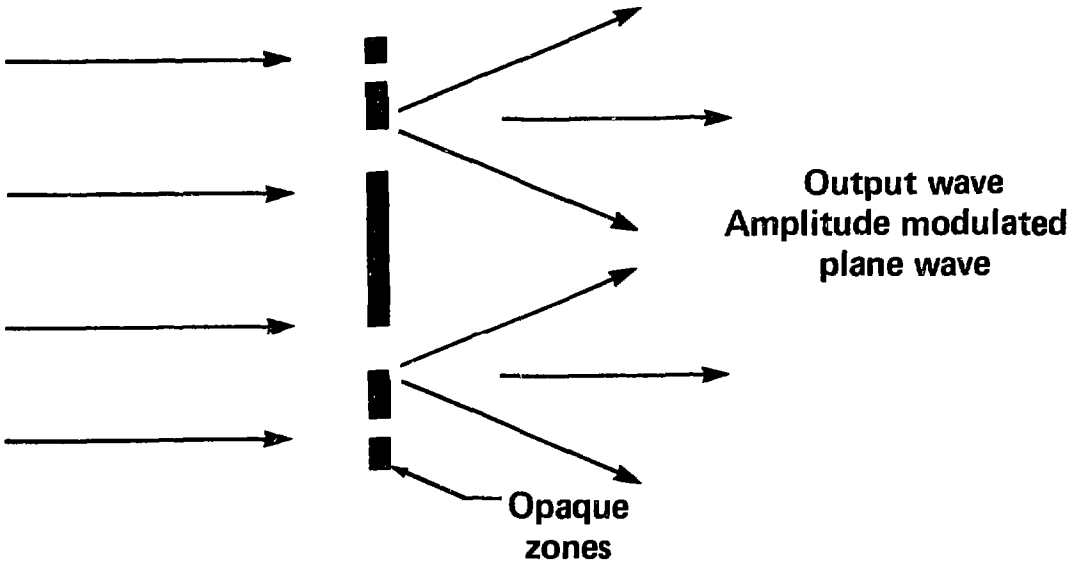

Fractional energy distribution

Device	1st order real focus	Absorbed	Undiffracted	All other foci
FZP	0.1	0.5	0.25	0.15

40-90-0877-1637

Fig. 7a

WHAT IS A BLAZED FRESNEL PHASE PLATE?

Illustration in stages: (2) Fresnel phase plate

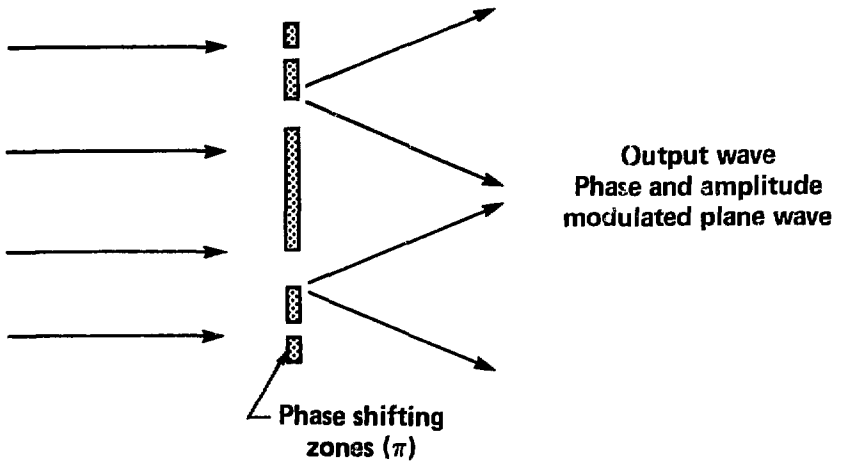

Fractional energy distribution*

Device	1st order real focus	Absorbed	Undiffracted	All other foci
FPP	$\left(\frac{1+\Gamma}{\pi}\right)^2$	$\left(\frac{1-\Gamma^2}{2}\right)$	$\left(\frac{1-\Gamma}{2}\right)^2$	$\frac{\pi^2-4}{4\pi^2}(1+\Gamma)^2$

*$\Gamma \equiv \exp(-\pi\eta)$ is the fractional amplitude transmission through a phase shifting zone of the FPP.

40-90-0877-1638

Fig. 7b

WHAT IS A BLAZED FRESNEL PHASE PLATE?

Illustration in stages: (3)

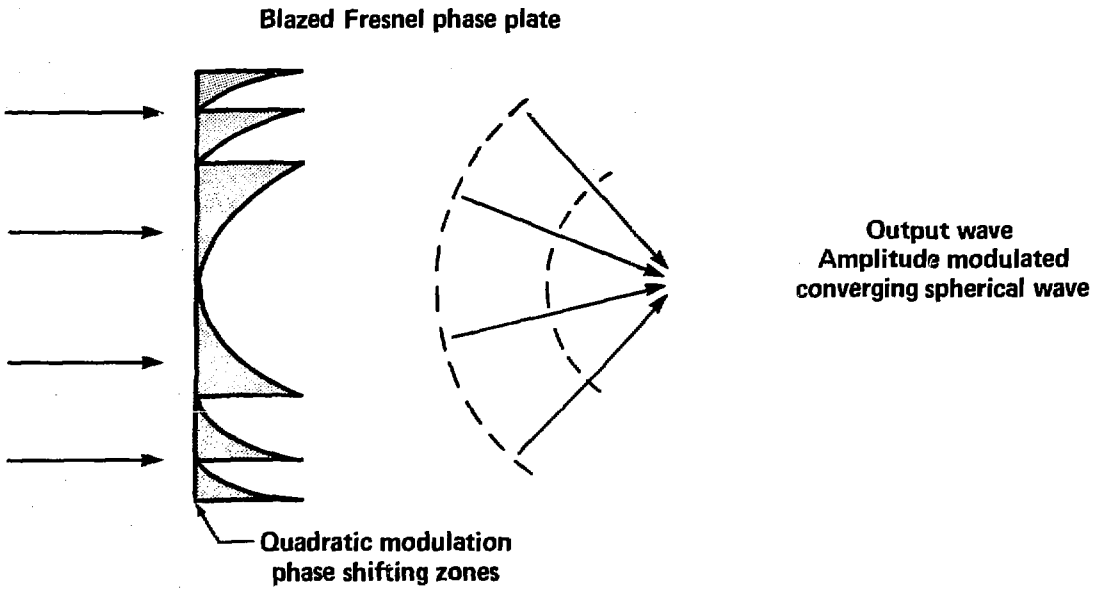

Fractional energy distribution*

Device	1st order real focus	Absorbed	Undiffracted	All other foci
BFPP	$\left(\frac{1-\Gamma^2}{2\pi\eta}\right)^2$	$1-\frac{(1-\Gamma^4)}{4\pi\eta}$	$\frac{\eta^2}{1+\eta^2}\left(\frac{1-\Gamma^2}{2\pi\eta}\right)^2$	$\frac{1-\Gamma^2}{2\pi\eta}\left(\frac{1+\Gamma^2}{2}-\frac{1+2\eta^2}{1+\eta^2}\cdot\frac{1-\Gamma^2}{2\pi\eta}\right)$

*$\eta \equiv k/\delta$; $\Gamma = \exp(-\pi\eta)$

40-90-0877-1639

Fig. 7c

4X ZONE PLATE (TEST) MICROSCOPE:

AL K_α radiation backlights a crude zone plate test pattern mask which is imaged using a 3200 Å linewidth zone plate "lens"

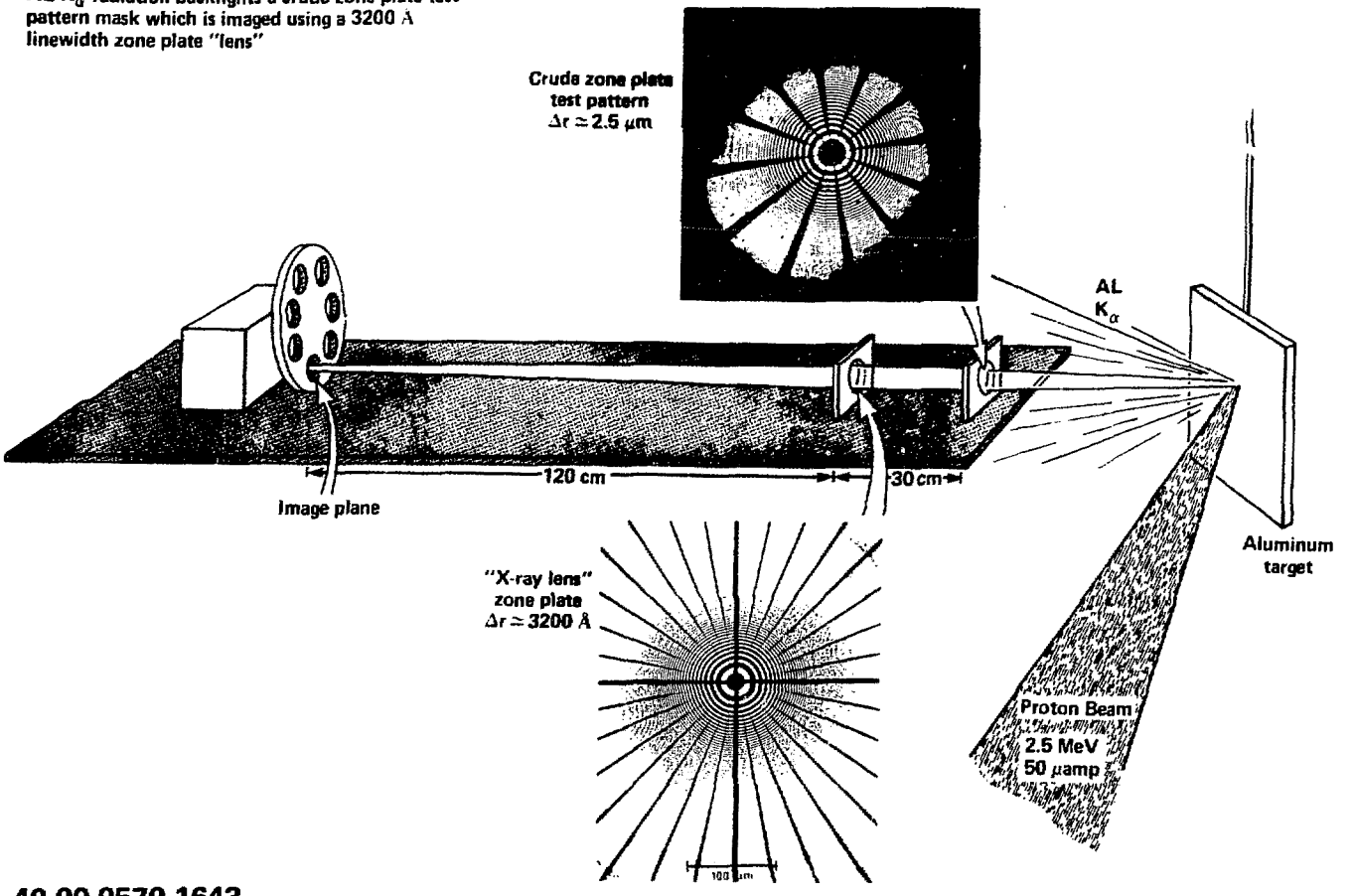

40-90-0579-1643

Fig. 8

ZONE PLATE "LENS" RESOLUTION TEST:

Initial results

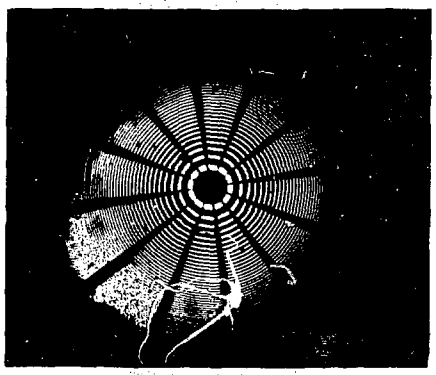

Test pattern
2.5 μm lines

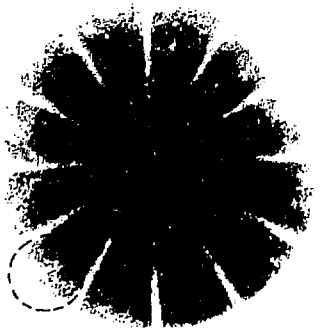

X-ray "lens" image

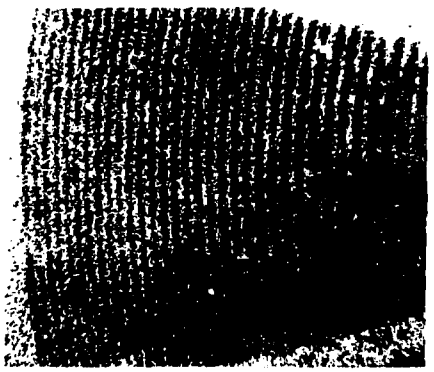

X-ray "lens" image
2.5 μm lines

40-90-0579-1644

Fig. 9

ZONE PLATE "LENS" RESOLUTION TEST:

Microdensitometer analysis of x-ray image:

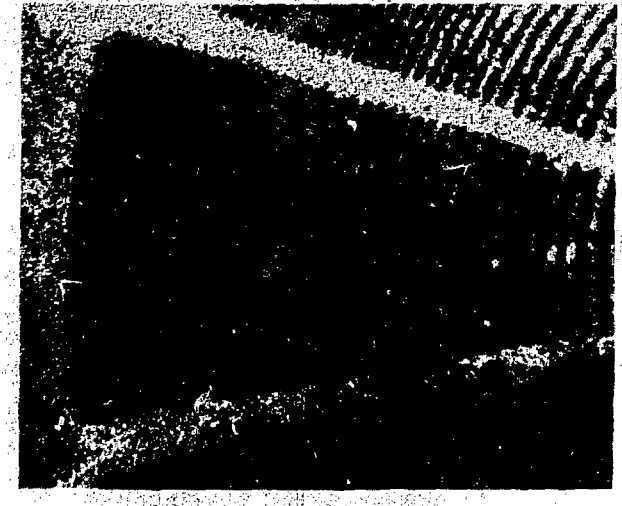

X-ray "lens" image

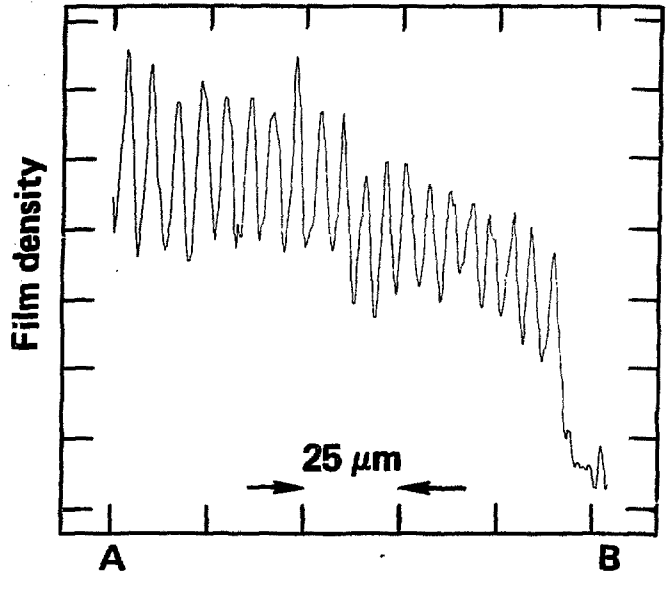

Conclude:

- **2.5 μm lines and spaces are clearly resolved**

40-90-0579-1645

Fig. 10

OFF-AXIS FRESNEL ZONE PLATE: IMAGING PROPERTIES

Definition:

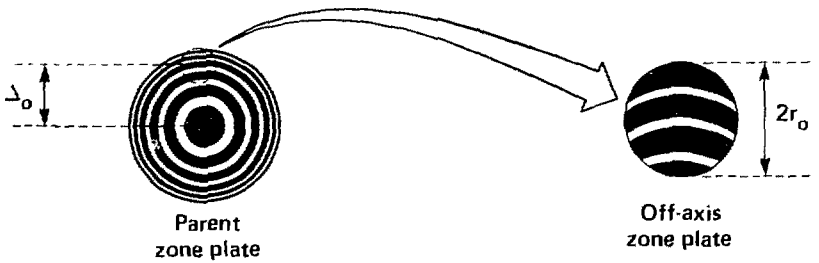

Imaging:

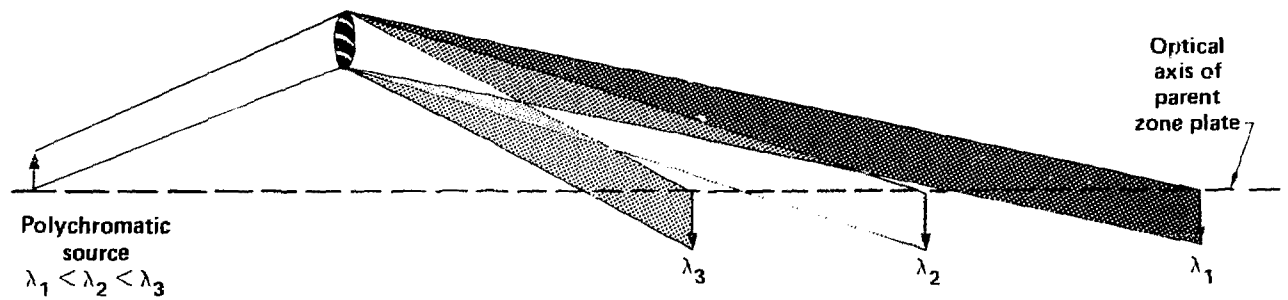

- Chromatically distinct emissions can be separated and individually imaged
- Focal length is that of parent zone plate
- Resolution and imaging characteristics are 'roughly' those of an on axis zone plate of the same linewidth and diameter

40-90-0579-1776

Fig. 11